Inorganic Chemistry

pubs.acs.org/IC

Article

Formation, Reactivity, and Catalytic Behavior of a Keggin Polyoxometalate/Bipyridine Hybrid in the Epoxidation of Cyclooctene with H_2O_2

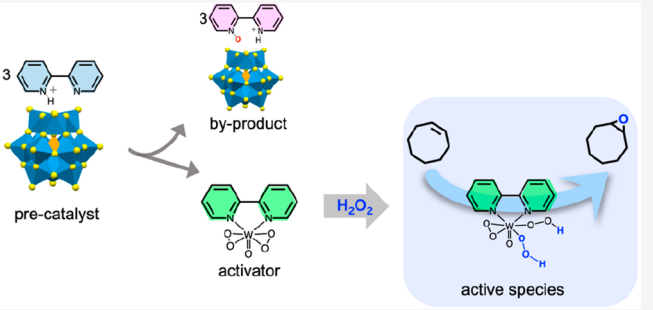
Gabriel Hidalgo, Gabriella Barozzino-Consiglio, Koen Robeyns, Michel Devillers, and Eric M. Gaigneaux*

Cite This: https://doi.org/10.1021/acs.inorgchem.3c00467

Read Online

ACCESS | Metrics & More | Article Recommendations | Supporting Information

ABSTRACT: The present study further explores the behavior of polyoxometalate-based hybrid compounds as catalysts for liquid-phase cyclooctene epoxidation with H_2O_2. Precisely, it unveils the nature of the relevant active species derived from the hybrid based on Keggin polyoxometalate (POM) and bipyridines (bpy) of formula $(2,2'\text{-Hbpy})_3[PW_{12}O_{40}]$ (**1**). Whereas (i) it is generally accepted that the catalytic oxidation of organic substrates by H_2O_2 involving Keggin HPAs proceeds via an oxygen transfer route from a peroxo intermediate and (ii) the catalytically active peroxo species is commonly postulated to be the polyperoxotungstate $\{PO_4[W(O)(O_2)_2]_4\}^{3-}$ complex (PW_4), we show that the studied epoxidation reaction seems to be more sophisticated than commonly reported. During the catalytic epoxidation, **1** underwent a partial transformation into two oxidized species, **2** and **3**. Compound **3** corresponding to 2,2′-bipyridinium oxodiperoxotungstate of formula $[WO(O_2)_2(2,2'\text{-bpy})]$ was shown to be the main species responsible for the selective epoxidation of cyclooctene since **2** (in which the POM is associated with a protonated mono-N-oxide derivative of 2,2′-bpy of formula $(2,2'\text{-HbpyO})_3[PW_{12}O_{40}]$) exhibited no activity. The structures of **1**, **2**, and **3** were solved by single-crystal X-ray diffraction and were independently synthesized. The speciation of **1** was monitored under catalytic conditions by ^{1}H and ^{1}H DOSY NMR spectroscopies, where the formation *in situ* of **2** and **3** was revealed. A reaction mechanism is proposed that highlights the pivotal, yet often underestimated, role of H_2O_2 in the reached catalytic performances. The active species responsible for the oxygen transfer to cyclooctene is a hydroperoxide intermediate species that is formed by the interaction between the anionic structure of the catalyst and H_2O_2. The latter operates as a "conservative agent" whose presence in the catalytic system is required to prevent the catalysts from deactivating irreversibly.



INTRODUCTION

Polyoxometalates (POMs) are discrete metal-oxide clusters composed of early transition-metal ions and oxo ligands.[1] Keggin heteropolyanions (HPAs) of general formula $[XM_{12}O_{40}]^{n-}$ (mainly M = Mo or W and X = P, Si, or Ge) are one of the most explored subsets of POMs in catalytic applications, particularly in the oxidation of organic substrates.[2−6] Much of the interest in these anions has emerged from their catalytic efficiency in oxidation reactions when combined with H_2O_2 as an oxidant. Relevant examples involve homogeneous[7,8,17−23,9−16] and heterogeneous oxidations[24−33] catalyzed by Keggin HPAs. One of the most successful routes to prepare active Keggin-based oxidation catalysts lies in the preparation of organic−inorganic hybrid materials. Typically, this is accomplished by combining Keggin HPAs with organic compounds, predominantly nitrogen-containing ligands. This method is, in fact, one of the most promising strategies in oxidation catalysis. The convenience of this method relies on the huge modularity, and therefore overall reactivity, provided by the organic−inorganic hybrid platform. Combining the intrinsic redox properties of the inorganic Keggin with those of the organic ligands (e.g., hydrophobic properties) has resulted in the development of novel functionalities relevant for catalytic applications, especially when combined with H_2O_2 for the epoxidation of olefins or oxidation of alcohols.[34−40] It is generally accepted that the catalytic oxidation of organic substrates by H_2O_2 involving Keggin HPAs proceeds via an oxygen transfer route from a peroxo intermediate (generated from the degradation of HPA with H_2O_2) to the olefin. The postulated catalytically active peroxo species is commonly

Received: February 12, 2023

Downloaded via UNIV CATHOLIQUE DE LOUVAIN on May 24, 2023 at 12:36:45 (UTC).
See https://pubs.acs.org/sharingguidelines for options on how to legitimately share published articles.

© XXXX American Chemical Society

reported as the polyperoxotungstate $\{PO_4[W(O)(O_2)_2]_4\}^{3-}$ complex (PW_4) that Venturello identified as the oxygen transfer agent derived from the catalytic oxidation itself.[9,11,18,20] In most cases, a large excess of H_2O_2 (with respect to the substrate) is used with the intention of "repairing" the catalyst's peroxo group after the oxygen transfer, thus making the process catalytic. These mechanistic studies are typically based on two theories postulated in the 1970s by Mimoun et al.[41,42] and Sharpless et al.,[43] which have been supported by later theoretical studies.[44] Nevertheless, as part of our continuous research on the catalytic and structural role of Keggin/bipyridine hybrids in the epoxidation of olefins with H_2O_2,[45,46] we show in the present study that the epoxidation reactions (specifically that of cyclooctene) seem to be more sophisticated than commonly reported. Herein, we disclose the identity of novel species derived *in situ* from the degradation of a Keggin/bipyridine hybrid with H_2O_2 during the cyclooctene epoxidation reaction. H_2O_2 is found to play an unusual role acting as both a conservative and oxygen transfer agent. This enabled us to derive a more accurate reaction mechanism which is crucial for rational optimization of the process.

EXPERIMENTAL SECTION

Materials. 2,2′-Bipyridine (2,2′-bpy) (99%) and *n*-hexane (96%) from TCI chemicals; hydrochloric acid (HCl, 37 wt %) and hydrogen peroxide (H_2O_2, 30 wt %) from Carl Roth; cyclooctene (C_8H_{14}, 95%), dibutyl ether ($C_8H_{18}O$, 99%, stabilized with BHT), and acetonitrile (C_2H_3N, for HPLC, isocratic grade) from VWR chemicals; *ortho*-phosphoric acid (H_3PO_4, 85%) from Merck; and cyclooctene oxide ($C_8H_{14}O$, 99%) and 2,2′-bipyridine N-oxide (98%) from Sigma-Aldrich were purchased and used as received. Phosphotungstic acid (PTA) was purchased from Sigma-Aldrich in the form of $H_3PW_{12}O_{40}{\cdot}xH_2O$ (reagent grade). Before further use, the fully hydrated PTA powder was placed under a vacuum (*ca.* 1.8×10^{-2} mbar) overnight at room temperature in order to evacuate its physisorbed water and obtain the hexahydrate form $H_3[PW_{12}O_{40}]{\cdot}6H_2O$.

Synthesis. *Synthesis of (2,2′-Hbpy)$_3$[PW$_{12}$O$_{40}$] (**1**).* To an aqueous mixture of PTA (1 mmol, 2.9881 g) in 9.5 mL of distilled water was added 2,2′-bpy (3 mmol, 0.4733 g), and it was magnetically stirred (500 rpm) for 1 h at room temperature. The resulting suspension was transferred to a sealed stainless-steel autoclave (70 mL) equipped with a Teflon jacket and heated to 120 °C for 5 h, then cooled to room temperature. The resulting white precipitate was filtered, rinsed several times with distilled water, and dried overnight under a vacuum (*ca.* 1.8×10^{-2} mbar) at room temperature.

*Preparation of Single Crystals of **1**.* Approximately 2 g of solid **1** is mixed with 28.5 mL of distilled water inside a sealed stainless-steel autoclave (70 mL) equipped with a Teflon jacket. The sealed system was then gradually heated over a period of 2 h from room temperature to 180 °C and then maintained at that temperature for 96 h. Subsequently, the system was gradually cooled to room temperature over a period of 18 h (10 °C h^{-1}) and maintained at that temperature for 8 h to allow crystallization.

Synthesis of Bipyridinium Salt. The synthesis was conducted according to the method previously described by our group.[46] Within the objective to probe the protonation state of the ligands in the hybrid, a fully protonated salt of 2,2′-bipyridine (2,2′-bpy; 99%) was prepared as reference material. To an aqueous solution of HCl (7.9 mL, 0.2 mol·L^{-1}) was added 0.0473 g of 2,2′-bpy (0.3 mmol), and it was magnetically stirred (500 rpm) for 1 h. The obtained solution was evaporated to dryness under a vacuum (*ca.* 1.8×10^{-2} mbar) overnight at room temperature. The obtained light pink colored solid was later stored in a desiccator for further characterization.

*Synthesis of (2,2′-HbpyO)$_3$[PW$_{12}$O$_{40}$] (**2**).* Compound **2** was synthesized based on the synthesis of compound **1** using the ligand 2,2′-bipyridine N-oxide (3 mmol, 0.5271 g).

*Synthesis of [WO(O$_2$)$_2$(2,2′-bpy)] (**3**).* A "direct" synthesis of **3** was carried out according to the method previously described by our group.[45] $H_3[PW_{12}O_{40}]{\cdot}6H_2O$ (1 mmol, 2.9881 g) was added to 30 wt % H_2O_2 (100 mmol, 10.2 mL). After reaction for 1 h at room temperature, H_3PO_4 (2 mmol, 135 μL) was added. After stirring (500 rpm) for 1 h, the solid ligand 2,2′-bpy (3 mmol, 0.4733 g) was added to the aqueous solution. The resulting suspension was stirred for 1 h, and the solid was then separated from the solution by filtration. The collected white particles were rinsed several times with water and dried overnight under a vacuum (*ca.* 1.8×10^{-2} mbar) at room temperature. Typically, 3.26 g of **3** is obtained along this synthesis corresponding to a yield of 64.7% (calculated on the basis of the amount of W engaged in the synthesis as Keggin acid vs that of W present in the particles of **3** recovered). In this case, however, the use of an autoclave is not needed to enhance crystallinity as was the case for **1** and **2**. More importantly, it is not recommended. If used, the peroxo groups of **3** decompose to oxygen, leading to uncontrolled production of O_2, resulting in pressure build-up and, thus, a possible explosion.

Precipitation of Dissolved Species. The precipitation procedure was conducted with the idea of studying the dissolved species that catalyze the reaction by characterization techniques in the solid state (e.g., PXRD, IR, Raman). This was accomplished by adding, after 24 h of catalytic reaction (under typical catalytic condition), *n*-hexane (610 μL) to a hot-filtrated mixture tested with or without H_2O_2 and leaving it stirring (500 rpm) overnight at 3 °C. Then, the obtained precipitated solid was separated by centrifugation (8000 rpm at 3 °C) and dried overnight under a vacuum (*ca.* 1.8×10^{-2} mbar) at room temperature. It is important to mention that centrifugation **must be** conducted at a low temperature (<15 °C) and rotational speeds of <8000 rpm. A small opening in the tube's cap must also be performed to decrease the pressure of the system during centrifugation. These precautions must be taken to prevent undesired explosions in the centrifugation tube due to the decomposition of peroxo groups, leading to uncontrolled production of O_2 and the accompanied pressure build-up.

Characterization of Samples. Single-crystal X-ray diffraction (SCXRD) was performed on a MAR345 image plate detector using Mo Kα (λ = 0.71073 Å) generated by a Rigaku Ultra X18S Rotating anode (FOX3D mirrors) or an Incoatec IμS microfocus source (focusing Montel multilayer optics ELM33). Suitable crystals were selected under an optical microscope and measured under ambient conditions or flash-cooled to the reported temperature. Data reduction was carried out using the CrysAlis^{PRO} software package. Structure solution and the refinement by full-matrix least-squares on F^2 have been performed using SHELXT and SHELX-2014/7, respectively. Non-hydrogen atoms were refined anisotropically; H atoms are added in calculated positions and allowed to ride on the parent atoms, with isotropic displacement factors set to 1.2 Ueq of the parent atoms (1.5 Ueq for methyl and OH hydrogens). Symmetry analysis and validation were carried out using PLATON. Pictures were made using the molecular visualization software Mercury 4.1.3.

CCDC 2231872−2231874 contain the supplementary crystallographic data for this paper. These data can be obtained free of charge from The Cambridge Crystallographic Data Centre via www.ccdc.cam.ac.uk/structures.

^{1}H NMR analyses were recorded at room temperature (295 K) on a Bruker Avance 500 operating at the Larmor frequency of 500 MHz. Experiments were run under TopSpin program (Bruker) using a BBO{^{1}H,X} probehead equipped with a *z*-gradient coil. ^{1}H DOSY NMR spectra were performed using the standard Bruker ledbpgp2s pulse program with gradient pulse periods (P30) of 0.7 ms and diffusion times (D20) of 100 ms. Gradient recovery delays of 150 ms followed the application of each gradient pulse. Data were systematically accumulated by linearly varying the diffusion encoding gradients over a range from 2% to 95% for 16 gradient increment values. The signal decay dimension on the pseudo-2D data was

https://doi.org/10.1021/acs.inorgchem.3c00467
Inorg. Chem. XXXX, XXX, XXX−XXX

generated by Fourier transformation of the time-domain data. Individual rows of the quasi-2D diffusion databases were phased and baseline corrected. Processing of NMR data were performed using Dynamics Center software (by Bruker supplier). Diffusion coefficients were calculated by fitting intensity data to the Stejskal-Tanner equation.

Powder X-ray diffraction (PXRD) patterns were recorded at room temperature on a Bruker-D8 Advance diffractometer (Bragg–Brentano geometry), equipped with a LYNXEYE XE-T detector, using Cu Kα radiation (λ = 0.15418 nm). The X-ray source was operated with a tension of 40 kV and a current of 30 mA. Diffractograms were collected between 5° and 80° (2θ) with 0.015° increments and 0.15 s per integration step. The sample was rotated at 5 rpm. All samples were analyzed using a Bruker silicon low background sample holder with a diameter of 20 mm. To aid the sample in adhering to the surface of the sample holder, a thin layer of a conventional cosmetic cream was applied prior to addition of the powder.

Raman spectra were recorded on a Bruker spectrometer (type RFS100/S) equipped with a liquid nitrogen detector and a Nd:YAG laser supplying the excitation line at 1064 nm with a power of 100 mW. The spectra were collected recording 32 scans in the range of 400 to 4000 cm^{-1} at 4 cm^{-1} in resolution and analyzed with OPUS software.

Fourier transform infrared spectra (IR) were recorded in a Bruker Equinox 55 with a DTGS detector equipped with a Bruker ATR platinum cell with a diamond crystal. The spectra were obtained by recording 500 scans from 400 to 4000 cm^{-1} with 4 cm^{-1} resolution in transmittance mode and analyzed by the software OPUS.

Thermogravimetric analysis–mass spectrometry (TGA-MS) was performed in a Mettler Toledo TGA/DSC 3+ apparatus coupled with a Pfeiffer Vacuum ThermoStar mass spectrometer. The samples were initially stabilized at 25 °C for 15 min and subsequently heated from 25 to 900 °C at 10 °C/min under synthetic air flow (50 mL/min, 80% N_2 and 20% O_2 Alphagaz 1 Air Liquide).

Catalytic Experiments. The catalytic tests were carried out at 70 °C under air in a closed 10 mL round-bottomed two-neck flask reactor equipped with a reflux condenser, oil bath, and magnetic stirring rod (500 rpm). Typically, the reactor was loaded with a catalyst (mass adjusted to 0.02 mmol of W atoms in the reactor); solvent CH_3CN (9.6 mL); internal standard dibutyl ether (1 mmol); 30 wt % aq. H_2O_2 (1 mmol); and cyclooctene (1 mmol). Before olefin addition, the reaction was preheated at the desired reaction temperature; the reaction time was counted immediately after olefin addition. The catalytic reaction was monitored every hour using a Shimadzu GC-2010 PLUS equipped with a capillary column (Shimadzu SH-Rtx-1 15 m × 0.25 mm) and a flame ionization detector. Assignments of reagents and products were made by comparison with authentic samples. Hot filtration tests, to explore the eventual occurrence of leaching of active species from the solids to the reaction liquid medium, were carried out under typical catalytic conditions for 2 h, after which the solid was separated from the reaction medium by filtration with a syringe equipped with a 0.2 μm VWR membrane filter. The remaining solution was subsequently monitored by GC at 70 °C.

RESULTS AND DISCUSSION

Synthesis and Characterization of Compound 1. Compound **1** was prepared by the hydrothermal reaction of phosphotungstic acid (PTA) and 2,2′-bpy in the molar ratio 1:3. Quantities were based on the measured pH (pH = 0.63) of the PTA solution and theoretical pK_a values of monoprotonated 2,2′-bpyH$^+$ (pK_{a2} = 4.4;[47] 4.5[48]) and diprotonated 2,2′-bpyH$_2^+$ (pK_{a1} = −0.2;[47] −0.5[48]) bipyridine species. The formation of **1** was confirmed by PXRD where new diffraction lines emerged from PTA and 2,2′-bpy precursors demonstrating the efficient integration of the precursor units in the crystal lattice (Supplementary Figure S1). Single crystals of **1** were prepared under a sealed autoclave system with controlled temperature gradients (see details in the Experimental Section) and analyzed by single-crystal X-ray diffraction (SCXRD). The SCXRD analysis confirmed the formula (2,2′-Hbpy)$_3$[$PW_{12}O_{40}$] for **1**.

Compound **1** crystallizes in the triclinic space group $P\bar{1}$ (table S1) and consists of a Keggin [$PW_{12}O_{40}$]$^{3-}$ (hereafter POM for short) anion surrounded by three protonated [2,2′-bpyH]$^+$ ligands (Figure 1a). The packing arrangement of **1**

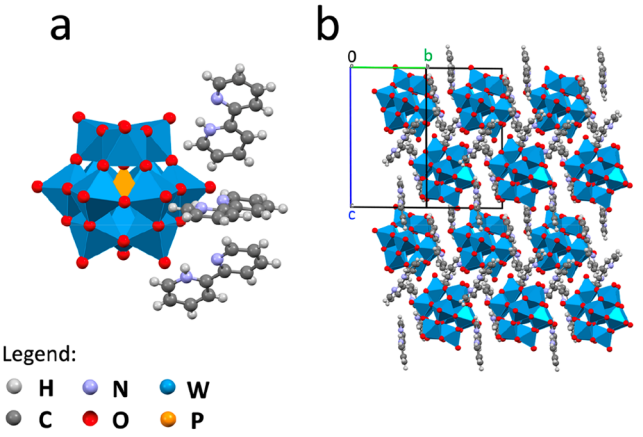


Figure 1. Polyhedral representation of **1** (a) and 3D view of the molecular packing between POM and bipyridine units in the *bc* plane (b).

(Figure 1b) shows isolated POM anions with the bipyridine cations hydrogen bonded to terminal oxygen atoms of the Keggin anion, through the N–H proton. One of the bipyridine cations bridges two Keggin anions in a bifurcated hydrogen bond interaction (see Table S4 for the list of hydrogen bond interactions and Figure S11 for a more detailed graphical representation). Characterization of the bulk material was performed to support the SCXRD data. TGA-MS confirmed that the stoichiometric POM/ligand ratio of **1** is 1:3 (Figure S2). The IR (4000–400 cm^{-1}) spectrum of **1** shows the presence of the Keggin anion[49,50] in the range of 1100–600 cm^{-1} and bipyridine[51] between 1660 and 1130 cm^{-1} (Figure S3). IR analysis comparing neutral 2,2′-bpy and a prepared fully protonated bipyridine salt (preparation details in Experimental Section) demonstrates that the hybridized bipyridines in **1** are protonated (Figure S4). This was based on the occurrence of bands at 1582 cm^{-1} due to ring stretching and 1620 cm^{-1} caused by N–H bending modes in **1**, similar to what is observed in the protonated ligand but not in neutral 2,2′-bpy.[52] The same comparative analysis was done using Raman where **1** exhibits stretching bands of pyridinium above 1600 cm^{-1} and pyridine at 1570 cm^{-1}, indicating that the ligands in **1** are monoprotonated *cis*-2,2′-bpyH$^+$ species[47,53,54] (Figure S5). A PXRD comparison of bulk **1** and respective simulated (S) patterns calculated from the SCXRD data shows excellent agreement (Figure 2). Therefore, the bulk analysis validates the formula (2,2′-Hbpy)$_3$[$PW_{12}O_{40}$] for **1** where three H$^+$ ions locate between the N atoms of bipyridine in *cisoidal*-conformation.

The structure of **1** is equivalent to the one reported by Yan et al., but in that case the compound is obtained from a more complex five-component association of $Na_2WO_4{\cdot}2H_2O$, powder metal W, H_3PO_4, $Mn(CH_3CO_2)_2$, and 2,2′-bpy.[55]

https://doi.org/10.1021/acs.inorgchem.3c00467
Inorg. Chem. XXXX, XXX, XXX–XXX

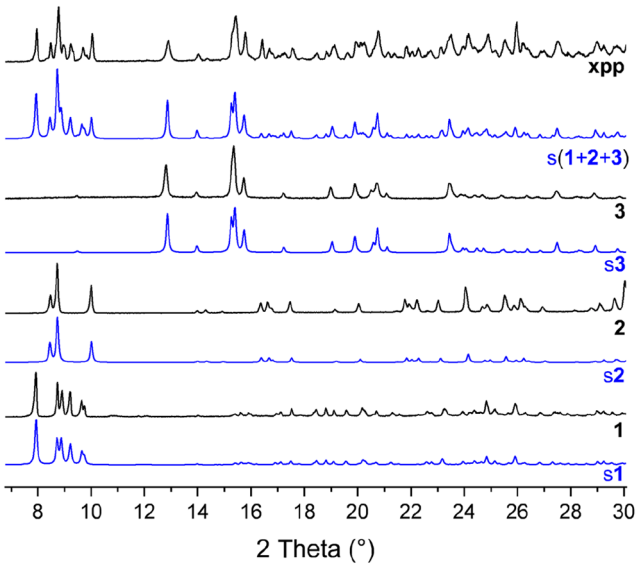


Figure 2. Simulated (S; blue) and bulk (black) PXRD patterns of compounds **1**, **2**, **3**, and xpp (which stands for unknown precipitate).

Catalytic Epoxidation of Cyclooctene with H_2O_2. Structural Identification of Species Derived from 1 during the Reaction. The catalytic properties of **1** were explored in the epoxidation of cyclooctene with H_2O_2. Little conversion was shown when the catalytic components were introduced in the sequence **1**/CH_3CN/H_2O_2/olefin (Table 1, entry 1), similar to the 5% conversion observed without catalyst. When **1** was exposed to H_2O_2 for 1 h before adding the olefin, the conversion slightly improved (Table 1, entry 2). Regardless of the addition order, **1** was shown to operate in the homogeneous phase as comparable activity was obtained after removing by filtration the apparent insoluble powder from the reaction mixture (Figure S6). Interestingly, when the hot filtration test (HFT) was applied, trace amounts of white solid particles labeled as xpp (where "x" stands for unknown, and "pp" refers to precipitate) were formed inside the reactor after 24 h of reaction (Scheme 1).

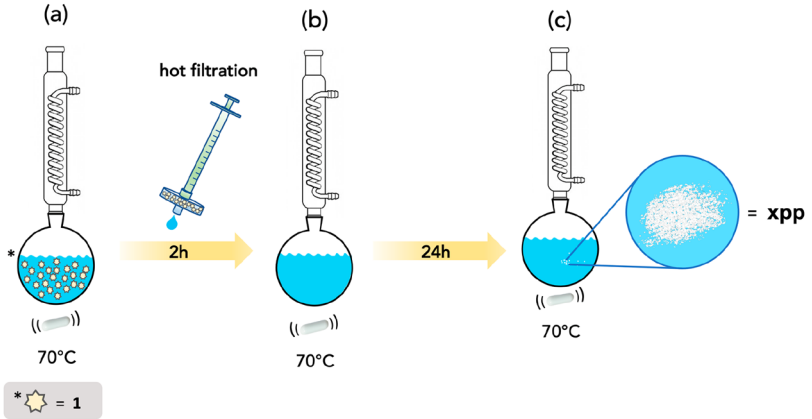
Table 1. Cyclooctene Epoxidation with H_2O_2 in the Presence of Either 1, 2, or 3[a]

entry	catalyst	conversion (%)
1	**1**/H_2O_2/cyclooctene	10
2	(**1**/H_2O_2) 1 h/cyclooctene	17
3	**2**	5
4	**3**	86
5	**3**/no H_2O_2[b]	14

[a]Reaction conditions: catalyst (0.02 mmol W), H_2O_2 (1 mmol), cyclooctene (1 mmol), 70 °C, 8 h. [b]H_2O_2 is not used. All tests showed 100% selectivity toward cyclooctene oxide.

To disclose the structural identity of xpp, single crystals for SCXRD analysis were prepared by gradually evaporating the filtrate catalytic mixture (i.e., after applying the hot filtration as depicted in step b of Scheme 1). This was achieved by transferring the filtrate from the reactor to a closed glass vessel equipped with a lid that was pierced with a syringe needle for gradual evaporation. The vessel was then placed in a dark environment at ambient temperature over a period of two months. During this time, three types of crystals were obtained, which formed at different rates, and subsequently analyzed by SCXRD. The SCXRD data revealed that one of the crystals corresponds to compound **1** (Figure 3). A second crystal, that crystallized in the rhombohedral space group *R*3*c* (Tables S2), consists of a novel hybrid in which a POM is associated with three protonated mono-N-oxide derivatives of 2,2′-bpy of general formula $(2,2'\text{-HbpyO})_3[PW_{12}O_{40}]$ (labeled as **2**; Figure 3). The POM is located on a 3-fold axis, and the central PO_4 is showing inversion disorder (58/42 ratio). The bipyridine rings are not entirely planar but are inclined about 16° from each other. While one nitrogen is oxidized (N−O), the other is protonated (N−H). Also, here disorder is observed on the nitrogens (N−O/NH), refining to a 53:47 ratio. The third crystal crystallized in the monoclinic space group $P2_1/n$ (Tables S3) and concerns an oxodiperoxo complex of formula $[WO(O_2)_2(2,2'\text{-bpy})]$ (labeled as **3**; Figure 3). The complex presents a W^{VI} center coordinated to two peroxo groups (O−O), one terminal oxo moiety (W═O), and a *N*,*N*′-chelated 2,2′-bpy ligand. The structure of **3** is isostructural to the one reported in 2015 by Amarante et al., where the complex is independently synthesized by reacting a tungsten oxide/2,2′-bpy hybrid of formula $[WO_3(2,2'\text{-bpy})]\cdot 2H_2O$ with H_2O_2 in

Scheme 1. Illustration of the Hot Filtration Protocol Carried out for 1[a]



[a]Step a depicts the reactor loaded with **1** in an apparent solid/liquid mixture; step b illustrates the homogeneous mixture after removal of solid **1**; step c shows precipitated white particles labelled xpp formed after 24 h from the homogeneous mixture.

https://doi.org/10.1021/acs.inorgchem.3c00467
Inorg. Chem. XXXX, XXX, XXX−XXX

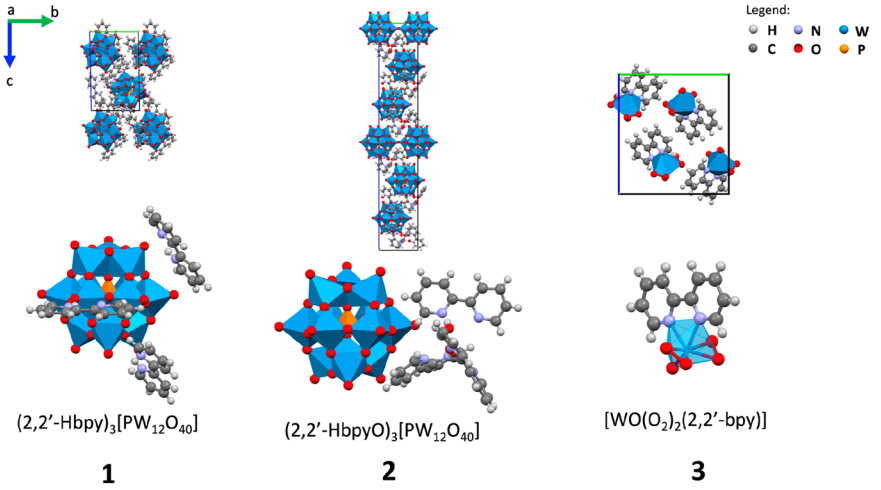


Figure 3. Mixed ball-and-stick and polyhedral representation of the crystal structures of **1**, **2**, and **3** (bottom). Above each hybrid is the crystal packing representation of the chain in the *ab* plane and respective unit cell.

CH_3CN,[56] which is also isotopical to the Mo^{IV} complex reported in 1984 by Schlemper et al.[57]

Based on the structural details obtained from SCXRD data, **2** and **3** were independently synthesized. Compound **2** was successfully obtained by hydrothermally reacting PTA with 2,2′-bipyridine N-oxide in water in a molar ratio of 1:3, identical to the procedure followed to prepare bulk **1**. The "direct" synthesis of **3** was also achieved on a relatively large scale by degrading PTA with H_2O_2 (see details in the Experimental Section). The diffraction profiles of bulk **2** and **3** vs their respective simulated patterns (i.e., **2** vs s**2** and **3** vs s**3** in Figure 2) show excellent agreement, demonstrating the successful synthesis of both compounds. IR analysis was also used to verify the identity of **2** and **3** (Figure S7). In the range of 1100−600 cm^{-1}, the presence of the POM structure in **2** is evidenced by the presence of bands of the phosphorus-bound oxygen (P−O), tungsten terminal oxygen (W═O_t), tungsten oxygen corner-sharing (W−O_c−W), and tungsten oxygen edge-sharing (W−O_e−W) bonds at 1076, 974, 892, and 754 cm^{-1}, respectively.[46] The presence of 2,2′-bipyridine N-oxide[58] is shown in the range of 1651−1143 cm^{-1} in which the N−O stretching mode appears at 1234 cm^{-1}. In the range of 1000−500 cm^{-1}, the oxodiperoxotungstate moiety of **3** is evidenced by the presence of stretching bands of groups W═O, O−O, and W(O_2) at 940, 830, and 538 cm^{-1}, respectively. The presence of bipyridine is shown in the range of 1650−1150 cm^{-1}. The coordination of bipyridine is manifested by the emergence of the ring stretching vibration of pyridyl rings at 1603 cm^{-1} exhibiting an intermediate character between protonated and neutral species.[45]

Dynamic Speciation Analysis of 1, 2, and 3. The precipitation process that leads to the formation of xpp from **1** was monitored by liquid-state 1D ^1H and 2D ^1H DOSY NMR spectroscopy. The idea of the analysis is to track the hybridized aromatic protons during precipitation, thus indirectly bringing information about the nature of the anionic part of the compounds. More precisely, it is aimed at following the chemical changes around the bipyridine environment from step B to step C of Scheme 1. Under catalytic conditions, the 1D ^1H NMR spectrum of the filtrate mixture, measured immediately after hot filtration (labeled as **1**, t = 2 h in Figure 4), shows a set of signals in the aromatic region from ca. 9 to

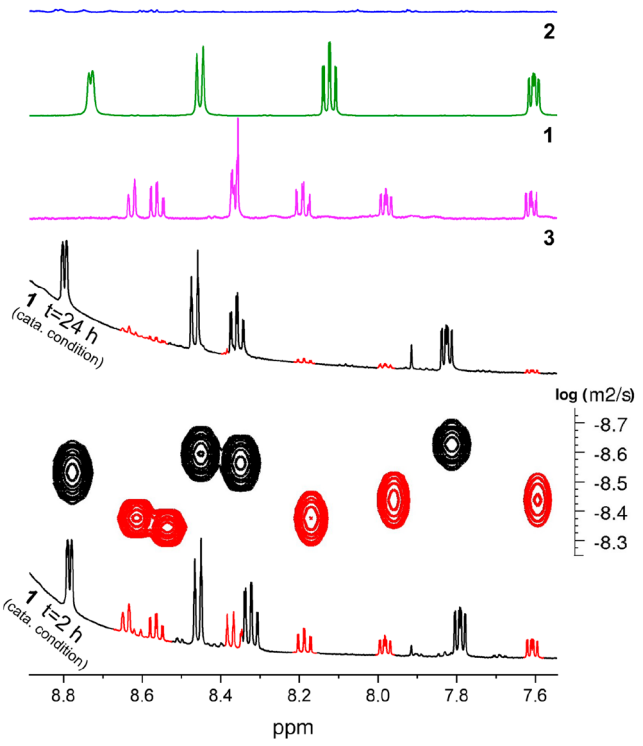


Figure 4. ^1H NMR spectra in CD_3CN of the filtrate mixture of **1** at time t = 2 h and after 24 h under typical catalytic conditions. The 2D DOSY ^1H NMR spectrum of the catalytic mixture at t = 2 h is shown between the two 1D ^1H NMR spectra. Red-colored peaks in the 1D and 2D spectra highlight the species that are consumed (precipitated) over time. The ^1H NMR spectra of bulk **3**, **1**, and **2** were prepared only in CD_3CN.

7.5 ppm. After 24 h, some of the signals of the mixture almost disappear (peaks marked in red from **1**, t = 2 h to t = 24 h) while others remain relatively unchanged (black peaks). We suggest that the species with resonance signals highlighted in red were precipitated and the ones in black remain in solution (solid white particles were observed to precipitate inside the NMR tube after 24 h). Note that the baseline of the spectra under catalytic conditions is not flat. This is due to the presence of H_2O_2 in the system, which generates a wide big

https://doi.org/10.1021/acs.inorgchem.3c00467
Inorg. Chem. XXXX, XXX, XXX−XXX

peak above 8.6 ppm. The 2D DOSY ^{1}H NMR spectrum of the reaction mixture at t = 2 h (red and black ovals in-between the two 1D spectra) revealed that, in the mixture, there are two main species with different diffusion coefficients. The faster-diffusing species (δ 8.63, 8.56, 8.36, 8.18, 7.98, and 7.60 ppm) presents an average diffusion coefficient of ca. 3.66×10^{-10} m^2 s^{-1} (red ovals), whereas the one that diffuses slowly (δ 8.78, 8.45, 8.32, and 7.79 ppm) has an average diffusion coefficient of ca. 2.36×10^{-10} m^2 s^{-1}. Hence, the DOSY spectrum indicates that the filtrate mixture contains two types of hybridized bipyridine species at t = 2 h. The species highlighted in red that eventually precipitates at t = 24 h is the smaller-sized molecule (diffuses faster than the one that remains in solution). To identify the nature of these hybridized bipyridine species, filtrated solutions of compounds **1**, **2**, and **3** in CD_3CN were independently prepared and subsequently analyzed by ^{1}H NMR.

The filtrates were obtained by making a saturated solution of the compound (0.5−1.0 g) with CD_3CN (5 mL) and stirring for 2 h at room temperature. Afterward, the suspension was filtered off and the filtrate was analyzed (Figure 4). The spectrum of **3** shows seven apparent resonance peaks in the aromatic region (ca. 7.61, 7.98, 8.20, 8.36, 8.56, 8.62, and 9.47 ppm). Integration of the signals with respect to the one at 9.47 ppm (peak shown in Figure S8) shows five signals with a 1:1 ratio (ca. 7.61, 7.98, 8.20, 8.56, 8.62 ppm) and one (8.36 ppm) with a 1:2 ratio, indicating that the spectrum of **3** contains eight aromatic protons in total (two of them overlap at a resonance of 8.36 ppm). The occurrence of eight protons agrees well with the unequivocal structure of **3** determined by SCXRD, demonstrating that those peaks correspond to an unsubstituted *N,N*-chelated 2,2′-bpy species. The resonance peaks of **3** match very well with the set of peaks consumed by precipitation in the catalytic mixture of **1** from t = 2 h to t = 24 h (red peaks). On the other hand, **1** (green spectrum) displays four apparent resonance peaks in the aromatic zone (ca. 7.60, 8.12, 8.45, and 8.73 ppm, and integrals approaching the 1:1:1:1 ratio, similar to 2,2′-bpy in Figure S8), which also shows good agreement with the solved structure of **1** where bipyridines appear as monoprotonated species in *cis* conformation electrostatically interacting with the POM. The presence of four equivalent protons of each hybridized pyridyl ring is then expected as it is typical for each aromatic proton of bipyridine.[59] In other words, each NMR peak integrates two protons due to the symmetry of bipyridine. These peaks moreover exhibit a multiplicity very similar to the NMR signals present in the catalytic mixture of **1** from t = 2 h to t = 24 h (peaks in black), suggesting that these peaks correspond to 2,2′-Hbpy$^+$ contained in **1**. The fact that the resonance frequencies of **1** are not the same as those that remained in solution at t = 24 h may be explained by the fact that **1** was prepared only in CD_3CN, whereas the filtrate catalytic mixture contains H_2O_2 and H_2O, causing shifts in the aromatic protons. These results are also in good agreement with the calculated diffusion coefficients of the species. Compound **3** diffuses faster (smaller size) than **1** (larger size).

However, according to the NMR results of Figure 4, only **3** appears to precipitate from the filtrate mixture after 24 h, which differs from the composition of the precipitate xpp (i.e., a mixture of **1**, **2**, and **3**). This can be explained by the fact that the ^{1}H NMR spectrum of **2** (in blue) exhibits very small, barely noticeable peaks in the aromatic region due to its poor solubility in acetonitrile. This suggests that as soon as **2** is formed during the catalytic reaction, it precipitates, making it unnoticeable in liquid-state ^{1}H NMR spectroscopy. On the other hand, the precipitation of **1** appears to occur in such a way that only a small fraction of the total solubilized portion precipitates, leaving most of solubilized **1** in solution.

Role of H_2O_2. Compounds **2** and **3** were individually tested in the epoxidation of cyclooctene with H_2O_2. Compound **2** showed no catalytic activity as it reached only 5% conversion (C) after 8 h, similar to that observed without a catalyst (Table 1, entry 3). Compound **3**, prepared along its "direct" synthesis, on the other hand, exhibited significantly higher conversion (86% C) under comparable catalytic conditions (Table 1, entry 4). These results suggest that the little conversion achieved by **1** after 8 h is most likely due to the presence of small amounts of active compound **3** produced throughout the catalytic reaction. The catalytic performance of **3** was also evaluated in the absence of H_2O_2. In this case, very low conversion is observed in comparison to when H_2O_2 is present in the reaction medium after 8 h (14% C vs 86% C). In both cases, **3** was shown to operate entirely in the homogeneous phase (see HFTs in Figure S9). As the reaction occurs in the homogeneous phase, attempts were made to isolate the soluble portion (dissolved active species) of compound **3** and then precipitate it in order to characterize the species in the solid state by Raman and PXRD. This was accomplished by adding *n*-hexane, after 24 h, to the hot-filtrated mixture tested with or without H_2O_2 (see Experimental Section). The collected solids were respectively labeled as "p**3**/H_2O_2-run1" for tests with H_2O_2 after the first catalytic run and "p**3**/noH_2O_2-run1" for those without H_2O_2, where the symbol "p" stands for "precipitation". PXRD analysis of the samples was conducted and compared to pristine **3** (Figure 5a). The

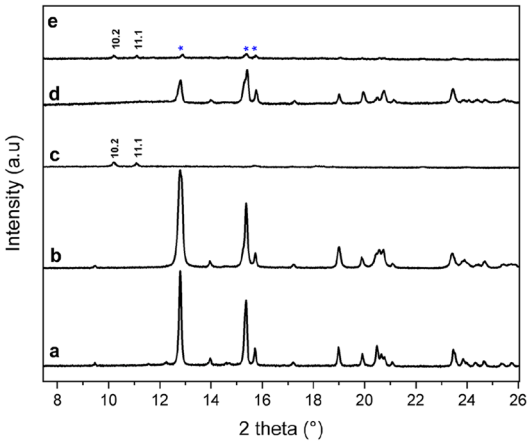


Figure 5. PXRD patterns of (a) **3**, (b) p**3**/H_2O_2-run1, (c) p**3**/noH_2O_2-run1 (d), p**3**/H_2O_2-run2, and (e) p**3**/noH_2O_2-run2. Symbol * indicates peaks of **3**.

diffractogram of p**3**/H_2O_2-run1 (Figure 5b) closely resembles that of pristine **3**, confirming that **3** retains its structure after the first catalytic run with H_2O_2. To the contrary, p**3**/noH_2O_2-run1 (Figure 5c) displays an overall amorphous phase with two small new and unknown peaks at a low angle (10.2° and 11.1°), indicating that **3** was structurally affected by the epoxidation when H_2O_2 was not present in the reaction medium. To test whether the damaged structure of **3**/noH_2O_2-run1 could be regenerated with fresh H_2O_2 and thus recover its

https://doi.org/10.1021/acs.inorgchem.3c00467
Inorg. Chem. XXXX, XXX, XXX−XXX

initial catalytic performance, the sample was tested in a second catalytic run with fresh H_2O_2.

The same catalytic test was also done for **3**/H_2O_2-run1 for comparison. To run the second catalytic tests, a hot-filtrated mixture of **3** was initially allowed to react in a first run with or without H_2O_2 for 24 h. Then, the filtrate containing soluble **3** was evaporated to dryness, leaving a pale-yellow residual paste. The reactor was then charged with fresh solvent, H_2O_2, and olefin, giving samples denoted respectively as **3**/H_2O_2-run2 and **3**/noH_2O_2-run2. Blank tests were also carried out to detect whether any amounts of olefin and/or epoxide were present in the residual paste after evaporating the solution from the first run. In this case, the residual paste was only mixed with solvent (10 mL of CH_3CN), stirred for 1 h, and then analyzed by GC. Only trace amounts of epoxide were detected, which were accounted for in the second run calculations. During the first 8 h, sample **3**/H_2O_2-run2 showed less activity than its first run **3**/H_2O_2-run1 (52% C vs 86%) but reached the same conversion values after 24 h (94% C; Figure 6). Conversely,

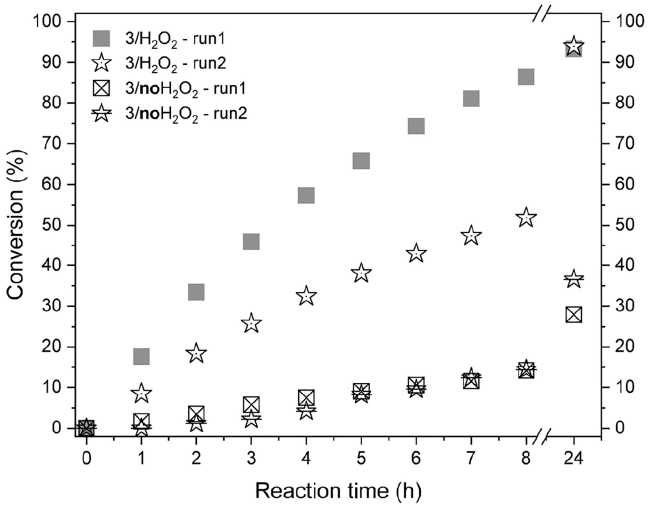


Figure 6. Epoxidation of cyclooctene catalyzed **3** with or without H_2O_2 after respective first and second catalytic runs (conditions in Table 1).

during the first 8 h, the activity of **3**/noH_2O_2-run2 did not improve and was the same as its first run **3**/noH_2O_2-run2 (14% C). Only a slight improvement in conversion was detected after 24 h (from 28% C to 37% C). To characterize the spent soluble species of **3** after the second run, the dissolved species were precipitated with *n*-hexane, using the same aforementioned procedure giving solids denoted as p**3**/H_2O_2-run2 and p**3**/noH_2O_2-run2. The diffraction patterns of p**3**/H_2O_2-run2 (Figure 5d) resemble those of its first run (Figure 5b) but with less intense peaks. On the other hand, the diffraction profile of p**3**/noH_2O_2-run2 (Figure 5d) closely resembles that of amorphous p**3**/noH_2O_2-run1 with the exception of the appearance of small diffraction peaks of crystalline **3**.

The fact that sample p**3**/H_2O_2-run2 shows relatively well-defined diffraction peaks compared to the overall amorphous profile of p**3**/noH_2O_2-run2,suggests that the structure of the latter was irreversibly damaged as a result of its initial run conducted without H_2O_2. The diffraction data also correlates well with the catalytic data shown in Figure 6. In all cases, the conversion decreases when precipitated **3** is less crystalline. For example, the modest catalytic improvement after 24 h of poorly active p**3**/noH_2O_2-run2 compared to its previous run p**3**/noH_2O_2-run1 is reflected by the appearance of small peaks of **3** (see * in Figure 5e) in the second run but not in the first one (Figure 5c). The activity/crystallinity relationship is likewise observed when **3** is permanently used with H_2O_2. The superior catalytic performance of the first run with respect to the second is linked to the better preservation of crystalline **3** species. To further evaluate whether the structural damage of p**3**/noH_2O_2-run2 could be reversed or not, an additional independent experiment was carried out. In this case, solid p**3**/noH_2O_2-run1 was allowed to react exclusively with an excess of H_2O_2 (1 mmol of H_2O_2 with respect to the molar mass of p**3**, which is less than the 0.02 mmol of W that was initially charged in the reactor) for 2 h at 70 °C to force its structural regeneration. After evaporation at room temperature under a vacuum overnight, the collected white solid was analyzed by PXRD. The obtained diffraction pattern closely resembles that of p**3**/noH_2O_2-run2, demonstrating that the structural regeneration is almost irreversible (Figure S10). In other words, the catalyst is permanently damaged if H_2O_2 is not used in the epoxidation. The precipitated samples were also analyzed by Raman and compared to pristine **3** (Figure 7a).

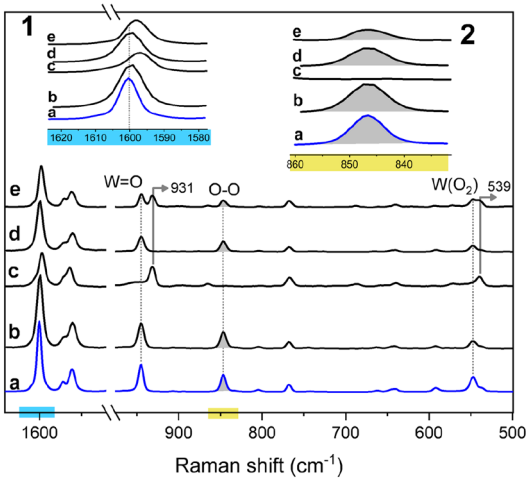


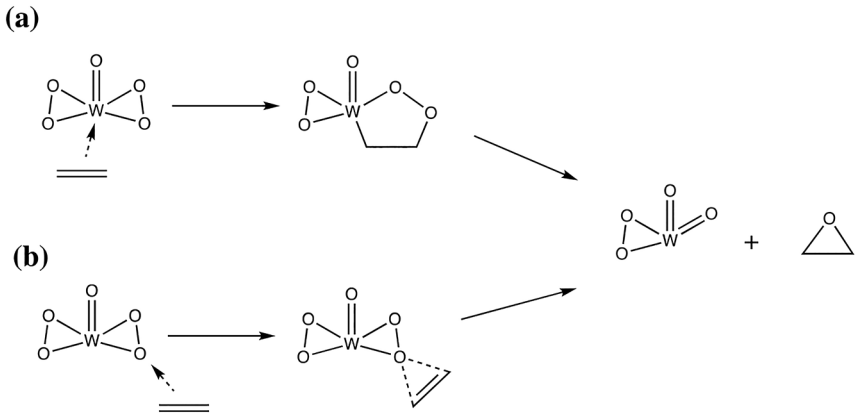
Figure 7. Raman spectra of (a) **3**, (b) p**3**/H_2O_2-run1, (c) p**3**/noH_2O_2-run1 (d), p**3**/H_2O_2-run2, and (e) p**3**/noH_2O_2-run2 in the mid- and low-frequency regions. Inset 1 depicts a zoomed view of the stretching vibrations of pyridyl rings, and inset 2 depicts peroxo O−O bands.

In the low-frequency region (*ca.* 1000−500 cm^{-1}), **3** shows bands at 945, 845, and 547 cm^{-1} due, respectively, to W═O, O−O, and W(O_2) groups.[45] The spectrum of p**3**/H_2O_2-run1 (Figure 7b) is very similar to that of pristine **3**, showing a well-defined band of its peroxo O−O groups (see zoomed comparison in Figure 7 inset 2, a vs b). On the other hand, p**3**/noH_2O_2-run1 appears different (Figure 7c).

The sample does not display peaks in the zone where bands of oxo and peroxo groups of **3** fall. Instead, it displays unknown bands at 931, 865, and 539 cm^{-1}. A closer look at the O−O vibrational region (inset 2c Figure 7) depicts a flat line proving the absence of peroxo groups in p**3**/noH_2O_2-run1. The appearance of unknown Raman bands in p**3**/noH_2O_2-run1 also coincides with the unknown diffraction peaks at a low angle (10.2° and 11.1°) observed in Figure 5c. The Raman profile of p**3**/H_2O_2-run2 (Figure 7d), on the other hand, resembles that of its first run and pristine **3** (see O−O groups

https://doi.org/10.1021/acs.inorgchem.3c00467
Inorg. Chem. XXXX, XXX, XXX−XXX

Scheme 2. Schematic Representation of the Two Possible Oxygen Transfer Routes for the Epoxidation of Olefins Catalyzed by Molybdenum(VI) or Tungsten(VI) Peroxo Complexes[a]



[a]Path a corresponds to the mechanism suggested by Sharpless,[43] and path b by Mimoun[41,42].

in inset 2 Figure 7) showing well-defined bands of W═O, O−O, and W(O_2) groups, in line with its structural preservation (Figure 5d). As expected, sample p**3**/noH_2O_2-run2 exhibits a combination of small bands of oxo and peroxo groups together with unknown ones showing that its structure is damaged (bands at 931, 865, and 539 cm^{-1}), and a fraction of it contains traces of crystalline **3** (little band of O−O groups, inset 2e Figure 7). When utilized without H_2O_2, the structural collapse of **3** also affects the vibrational frequency of bipyridine. For example, in the midfrequency region (*ca.* 1610−1580 cm^{-1}), the pyridyl rings of pristine **3** vibrate at 1600 cm^{-1}. However, the position of the band moves toward lower frequencies as the structural damage of **3** increases. In the case of the most structurally affected p**3**/noH_2O_2-run1, the band moves from 1600 cm^{-1} (pristine **3**) to 1596 cm^{-1} (see inset 1, Figure 7).

In summary, the absence of H_2O_2 in the reaction medium appears to have a detrimental catalytic and structural effect on compound **3**. The amorphous structure of p**3**/noH_2O_2-run1 together with the unknown Raman bands of its inorganic skeleton indicate that its anionic W$(O_2)_2$ structure was completely altered. Specifically, the absence of peroxo O−O bands and vibration of the bipyridine toward lower frequencies suggest that **3** gradually spent all its active structural oxygens at the end of the catalytic reaction (24 h). Due to this, the atomic bonding environment of tungsten in the **W**$(O_2)_2$ sphere likely changed, inducing a rearrangement of W−O bonds in a less ordered pattern. This presumably led to its amorphous structure and unknown skeletal bands in the low-frequency region of the Raman spectrum. Furthermore, the shift of the pyridyl rings toward lower frequencies (from 1600 to 1597 cm^{-1}) confirms the alteration of the ligand/anion coordination sphere, likely due to a change in the overall anionic charge of the cluster. The situation persisted even when the structurally affected p**3**/noH_2O_2-run1 was allowed to react exclusively with an excess of H_2O_2 for 2 h at 70 °C to force its structural regeneration, demonstrating that the process is almost irreversible and that the catalyst is permanently damaged if H_2O_2 is not used in the epoxidation. This was not the case for sample p**3**/H_2O_2-run1. Its PXRD and Raman profiles, which are close to that of pristine **3**, prove that during the epoxidation, H_2O_2 could efficiently regenerate its peroxo (W$(\mathbf{O_2})_2$) groups and hence retain its overall structure.

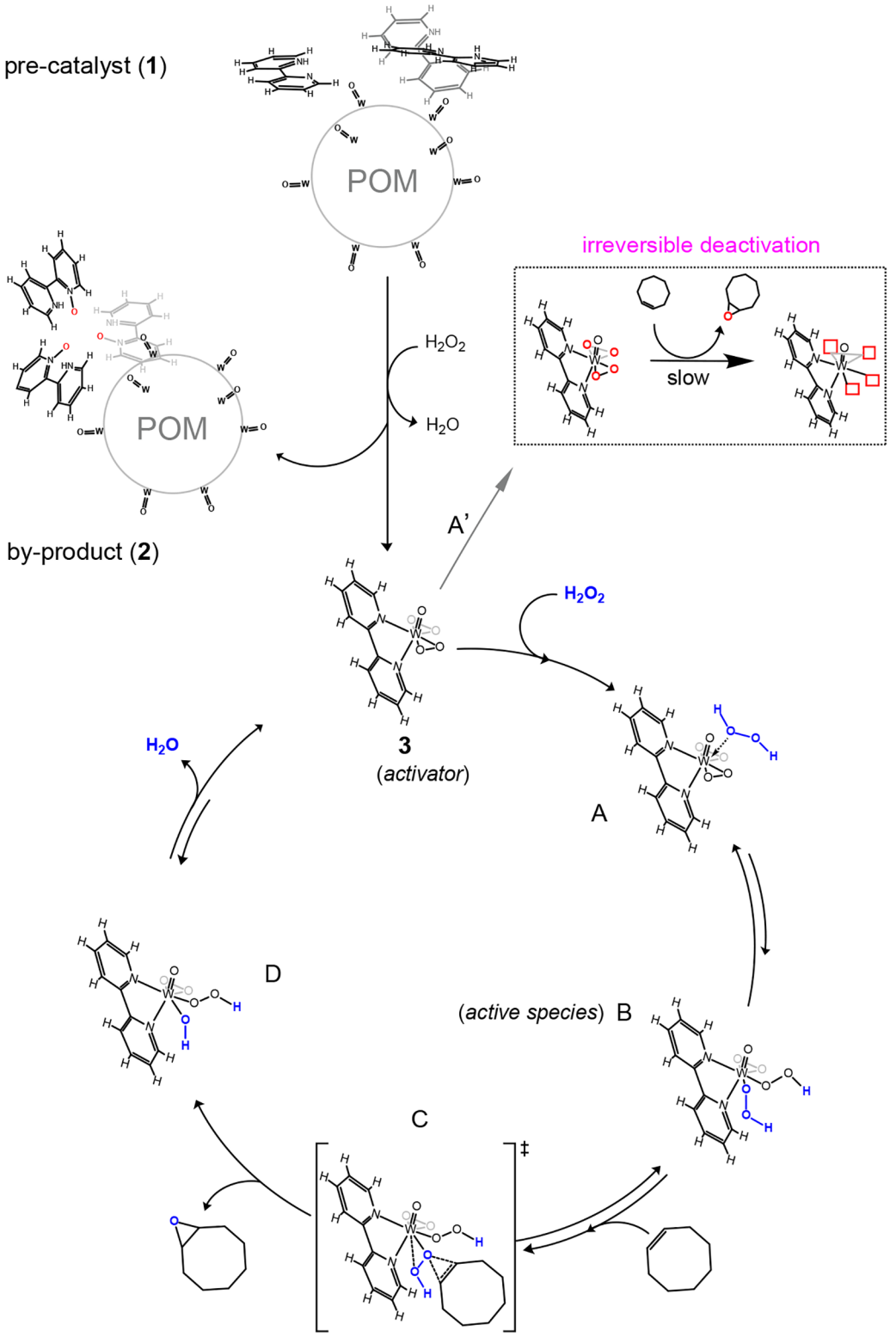
Mechanism of the Epoxidation. All of these findings, as well as a better understanding of the catalytic process involving compounds **1**, **2**, and **3**, open new questions from a mechanistic point of view. In fact, the mechanism of the reaction, which is of the utmost importance for rational optimization of the process, has been the subject of an unresolved controversy for decades.[60] The first suggestion of the possible oxygen transfer process was made by Mimoun et al. in 1970.[41,42] In this mechanism, the author proposes a multiple-step reaction process.

The first step involves the coordination of the olefin to the metal followed by the formation of a five-membered peroxo-metallocyclic adduct (Scheme 2a). The epoxide is then released by a cycloreversion reaction leaving a metal oxide species that further reacts with H_2O_2 to form the fresh peroxo complex in a catalytic cycle. Alternatively, in 1972, Sharpless et al.[43] suggested a direct nucleophilic attack of the olefin on the electrophilic peroxo ligand via a "butterfly" transition state (Scheme 2b). In recent years, these long-lasting mechanistic representations based on kinetic studies have been further addressed by theoretical studies. According to the theoretical calculations, the epoxidation proceeds in a single-step reaction via direct attack of the nucleophilic olefin to an electrophilic peroxo oxygen as the one proposed by Sharpless et al.[44] They also concluded that a mechanism via a five-membered metallacycle adduct, as proposed by Mimoun et al., is unfavorable. In our case, however, none of the mechanisms reflect our catalytic results. For example, in our case, the conversion of **3** at 1 h/3 h leads to 18%/46% when H_2O_2 is present in the reaction medium. However, when H_2O_2 is not present, the same reaction at 1 h/3 h shows conversion values of 2%/6% (Figure 6). Based on the mechanisms proposed by Mimoun et al., Sharpless et al., and theoretical studies, the oxygen that is transferred to the olefin comes from the peroxo ligand η^2-coordinated to tungsten (Scheme 2a,b).

Therefore, if the complex is the one that transfers the oxygen atom to the olefin, and such a complex is subsequently "repaired" by H_2O_2 during the epoxidation reaction, then the conversion evolution with **3** conducted without H_2O_2 should display a different profile. For instance, one would expect a conversion profile somewhat similar to that of a catalytic solution after a hot filtration test, where the solid catalyst is removed after 2−3 h to validate its heterogeneous nature. In

https://doi.org/10.1021/acs.inorgchem.3c00467
Inorg. Chem. XXXX, XXX, XXX−XXX

Scheme 3. Proposed Reaction Mechanism (Based on Literature Data[61,62]) for Epoxidation of Cyclooctene with H_2O_2 Catalyzed by 3[a]



[a]The drawings are based on the SCXRD data and so represent genuine structures. For the sake of clarity, the real PW_{12} structure was replaced, at the same position, by a circle.

other words, a rapid oxygen transfer to the olefin at the beginning of the reaction was followed by a nearly constant horizontal conversion line due to the lack of repaired peroxo complex. If the rate of the epoxidation depends on how many "dissolved" peroxo complexes are available in the reactor, then the conversion of **3** without H_2O_2 at early stages (i.e., 1 h/3 h)

https://doi.org/10.1021/acs.inorgchem.3c00467
Inorg. Chem. XXXX, XXX, XXX−XXX

should be close to 18%/46% and not 2%/6%. Furthermore, we proved that when the peroxo groups of **3** are completely spent after a 24 h catalytic run, the structure cannot be regenerated back to its original form when reacting with excess H_2O_2. In fact, the spent **3** structure is irreversibly degraded. However, it appears that when H_2O_2 participates in the epoxidation, it not only could, presumably, restore the spent peroxo groups of the complex but, rather, it seems to accelerate the catalytic epoxidation. Therefore, the above-proposed mechanisms are inconsistent with our catalytic and spectroscopic data. In fact, the central question resides in whether **3** functions as the effective active species or as a catalyst precursor.

A more consistent mechanism supported by spectroscopic studies and kinetic data was reported by Thiel et al.[61,62] The authors used a series of synthesized oxodiperoxo molybdenum complexes chelated with pyrazolylpyridine ligands as catalysts in the epoxidation of olefin with *t*-BuOOH or H_2O_2. The study concluded that the complexes do not catalyze the olefin epoxidation by transferring an oxygen atom of a peroxo ligand but by activating H_2O_2, which gives rise to a new reaction mechanism. Inspired by the coherence of this mechanism with our spectroscopic and catalytic observations, as well as the unequivocally solved structures derived from the epoxidation reaction, a reaction mechanism for the epoxidation of cyclooctene with H_2O_2 catalyzed by **3** is proposed (Scheme 3). In the first step, compound **1**, which acts as a precatalyst, is degraded by H_2O_2 producing the catalytically inactive N-oxide PW_{12} derivative **2** and the oxodiperoxo compound **3**. Then, the oxidizing agent H_2O_2 coordinates to the Lewis-acidic W(VI) center (A) followed by a proton transfer from coordinated H_2O_2 to one of the η^2-peroxo ligands of **3** (B). η^2-Coordination to tungsten activates the hydroperoxo ligand (highlighted in blue) derived from H_2O_2 (C). The epoxidation then occurs via an O-atom transfer from the active hydroperoxo ligand site to the olefin. The resulting alcoholato (W−O−H) ligand (D) abstracts the proton from the hydroperoxo group, which regenerates the diperoxo complex **3**. Therefore, based on this mechanism, **3** would function as an "activator" of the oxidizing agent H_2O_2 and compound B would act as the true active species. Hence, coordination of the Lewis-acidic metal center plays a central role in the activation of the hydroperoxide ligand and thus the epoxidation activity. The *N*,*N*′-chelating effect of 2,2′-bpy to the W^{VI} center is also assumed to play a role in the coordination step, according to previous studies of our group.[45,46] Based on the logic of this mechanism, a more elaborated argument for the catalyst deactivation can be derived. At this point, it is evident that, in addition to the kinetically competent reaction catalyzed by the oxidizing agent, which is activated by the peroxo complex, there is also an oxygen transfer, albeit kinetically less relevant, derived from the η^2-peroxo ligands of the **3** structure itself (step A′ and dotted box in Scheme 3). In other words, there are two parallel catalytic events taking place during the epoxidation reaction. One is where H_2O_2 is rapidly spent *via* the activator-complex route. This one is the most catalytically relevant process in the epoxidation. The second event involves the direct epoxidation of the olefin, which occurs at a much slower rate, by the peroxo oxygen atoms in **3**. The structure of which is later damaged after the oxygen transfer. Therefore, the catalytic inactivation occurs because H_2O_2 cannot coordinate with the damaged structure of **3** anymore. In other words, the conversion decreases because the population of fresh **3** species in the reaction mixture, namely the key for the activation of H_2O_2, reduces irreversibly with time.

CONCLUSION

Compound **1** of formula $(2,2'\text{-Hbpy})_3[PW_{12}O_{40}]$ was shown to generate *in situ* two oxidized compounds of formulas $(2,2'\text{-bpyHO})_3[PW_{12}O_{40}]$ (**2**) and $[WO(O_2)_2(2,2'\text{-bpy})]$ (**3**) in the epoxidation of cyclooctene with H_2O_2. The poor epoxidation activity of **1** was related to the little amount of **3** produced throughout the reaction. When "directly" synthesized (i.e., not from **1**) on a relatively large scale and tested in the epoxidation, **3** was the only catalytically relevant species as **2** was shown to be inactive. When **3** is tested without H_2O_2, the epoxidation activity and the structure of the catalyst are highly compromised, but not when H_2O_2 is present. Apart from hardly catalyzing the epoxidation, the lack of H_2O_2 in the system leaves the structure of **3** irreversibly damaged, rendering it ineffective for further use. Even when the broken catalyst is heated and mixed exclusively with an excess of H_2O_2, the structure remains amorphous along with a totally altered anionic $WO(O_2)_2$ skeleton. Based on the gathered data, a reaction mechanism was proposed which was shown to be coherent with our spectroscopic and catalytic evidence. In this case, the presumably catalytically active species **3** does not catalyze the cyclooctene epoxidation by transferring a peroxo oxygen atom from its structure but by activation of H_2O_2 which gives rise to a new catalytically active hydroperoxide species. Based on this mechanism, it was postulated that the deactivation of the catalyst is due to the irreversible loss of **3** peroxo groups throughout the catalytic process which are unable to activate H_2O_2 and generate the active hydroperoxide species required to catalyze the epoxidation. Finally, the formation, speciation, and reactivity aspects covered here are helpful to design and develop potential heterogeneous catalytic systems that incorporate Keggin POMs or oxodiperoxotungstate catalysts based on bipyridine or any other equivalent ligand. At this stage of the study, after having elucidated the nature of the active species and its reaction mechanism in the epoxidation of cyclooctene, it would be interesting to validate the here reported findings in the case of other olefins. Also addressing the scale-up of the "direct" preparation of the active species, namely **3**, even more than what has been achieved here, and improving its yield, would be interesting. As the "direct" synthesis protocol of **3** proposed here does not imply complicated unit operations nor hazardous/expensive chemicals, one can be optimistic. In this regard, a preliminary alternative to the synthesis protocol of **3** described here may be found in ref 63.

ASSOCIATED CONTENT

Supporting Information

The Supporting Information is available free of charge at https://pubs.acs.org/doi/10.1021/acs.inorgchem.3c00467.

PXRD patterns (Figure S1) of **1** and precursors; crystal data (Table S1) of **1**; crystal data (Table S2) of **2**; crystal data (Table S3) of **3**; TGA-MS profile (Figure S2) of **1** and PTA; IR spectra (Figure S3) of **1** and PTA; IR spectra (Figure S4) of **1**, neutral and protonated bipyridine in mid- and high-frequency regions; Raman spectra (Figure S5) of **1**, neutral and protonated bipyridine; conversion profile (Figure S6) of **1** and respective hot filtration tests; IR spectra (Figure S7) of **2**

https://doi.org/10.1021/acs.inorgchem.3c00467
Inorg. Chem. XXXX, XXX, XXX−XXX

and 3; ^{1}H NMR spectra (Figure S8) of **1**, **2**, **3**, and 2,2′-bpy; conversion profile (Figure S9) of **3** with and without H_2O_2 and respective hot filtration tests; PXRD patterns (Figure S10) of precipitated **3** with and without H_2O_2 after the first and second catalytic runs (PDF)

Accession Codes

CCDC 2231872−2231874 contain the supplementary crystallographic data for this paper. These data can be obtained free of charge via www.ccdc.cam.ac.uk/data_request/cif, or by emailing data_request@ccdc.cam.ac.uk, or by contacting The Cambridge Crystallographic Data Centre, 12 Union Road, Cambridge CB2 1EZ, UK; fax: +44 1223 336033.

AUTHOR INFORMATION

Corresponding Author

Eric M. Gaigneaux − *Institute of Condensed Matter and Nanosciences (IMCN), Université catholique de Louvain (UCLouvain), 1348 Louvain-la-Neuve, Belgium;* orcid.org/0000-0003-2239-4306; Email: eric.gaigneaux@uclouvain.be

Authors

Gabriel Hidalgo − *Institute of Condensed Matter and Nanosciences (IMCN), Université catholique de Louvain (UCLouvain), 1348 Louvain-la-Neuve, Belgium;* orcid.org/0000-0001-5804-2850

Gabriella Barozzino-Consiglio − *Institute of Condensed Matter and Nanosciences (IMCN), Université catholique de Louvain (UCLouvain), 1348 Louvain-la-Neuve, Belgium*

Koen Robeyns − *Institute of Condensed Matter and Nanosciences (IMCN), Université catholique de Louvain (UCLouvain), 1348 Louvain-la-Neuve, Belgium;* orcid.org/0000-0002-4763-4217

Michel Devillers − *Institute of Condensed Matter and Nanosciences (IMCN), Université catholique de Louvain (UCLouvain), 1348 Louvain-la-Neuve, Belgium*

Complete contact information is available at: https://pubs.acs.org/10.1021/acs.inorgchem.3c00467

Notes

The authors declare no competing financial interest.

ACKNOWLEDGMENTS

The authors acknowledge the "Communauté Franćaise de Belgique" for the financial support through the ARC programme (15/20-069) and the purchase of the equipment thanks to F.N.R.S. (projects CDR J.0156.18 for DRUV and EQP U.N006.16 for PXRD).

REFERENCES

(1) Vilà-Nadal, L.; Mitchell, S. G.; Markov, S.; Busche, C.; Georgiev, V.; Asenov, A.; Cronin, L. Towards Polyoxometalate-Cluster-Based Nano-Electronics. *Chem. - A Eur. J.* **2013**, *19* (49), 16502−16511.

(2) Proust, A.; Thouvenot, R.; Gouzerh, P. Functionalization of Polyoxometalates: Towards Advanced Applications in Catalysis and Materials Science. *Chem. Commun.* **2008**, No. 16, 1837.

(3) *Liquid Phase Oxidation via Heterogeneous Catalysis*; Clerici, M. G., Kholdeeva, O. A., Eds.; John Wiley & Sons, Inc.: Hoboken, NJ, 2013.

(4) Song, Y. F.; Tsunashima, R. Recent Advances on Polyoxometalate-Based Molecular and Composite Materials. *Chem. Soc. Rev.* **2012**, *41* (22), 7384−7402.

(5) Ma, Y.; Jiang, Y.; Wei, X.; Peng, Q.; Dai, S.; Hou, Z. Hydrocarboxylation of Olefins Catalyzed by Polyoxometalate-Anchored Palladium Single-Atom Catalysts. *ACS Sustain. Chem. Eng.* **2022**, *10* (47), 15389−15401.

(6) Liu, J.; Huang, M.; Hua, Z.; Dong, Y.; Feng, Z.; Sun, T.; Chen, C. Polyoxometalate-Based Metal Organic Frameworks: Recent Advances and Challenges. *ChemistrySelect* **2022**, *7* (18), e202200546.

(7) Sun, J.; Zhao, X.; Sun, G.; Zeb, S.; Cui, Y.; You, Q. Thermodynamic and Kinetic Study on the Catalytic Epoxidation of Allyl Chloride with H2O2 by New Catalyst $[(C_{18}H_{37})_2(CH_3)_2N]_3\{PO_4[W(O)(O_2)_2]_4\}$. *Chem. Eng. J.* **2020**, *398* (April), 125051.

(8) Zhao, X.; Sun, J.; Sun, G.; You, Q.; Jiang, X.; Cui, Y. Epoxidation of Allyl Chloride with H_2O_2 Catalyzed by Three Structurally Related Quaternary Ammonium Modified Polyoxophosphotungstates. *Appl. Catal. A Gen.* **2020**, *608* (May), 117846.

(9) Venturello, C.; D'Aloisio, R.; Bart, J. C. J.; Ricci, M. A New Peroxotungsten Heteropoly Anion with Special Oxidizing Properties: Synthesis and Structure of Tetrahexylammonium Tetra-(Diperoxotungsto)Phosphate(3-). *J. Mol. Catal.* **1985**, *32* (1), 107−110.

(10) Schmidt, F.; Cokoja, M. Supramolecular Concepts for the Biphasic Epoxidation of Olefins Using Aqueous Hydrogen Peroxide. *Green Chem.* **2021**, *23* (2), 708−722.

(11) Venturello, C.; Alneri, E.; Ricci, M. A New, Effective Catalytic System for Epoxidation of Olefins by Hydrogen Peroxide under Phase-Transfer Conditions. *J. Org. Chem.* **1983**, *48* (21), 3831−3833.

(12) Pai, Z. P.; Chesalov, Y. A.; Berdnikova, P. V.; Uslamin, E. A.; Yushchenko, D. Y.; Uchenova, Y. V.; Khlebnikova, T. B.; Baltakhinov, V. P.; Kochubey, D. I.; Bukhtiyarov, V. I. Tungsten Peroxopolyoxo Complexes as Advanced Catalysts for the Oxidation of Organic Compounds with Hydrogen Peroxide. *Appl. Catal. A Gen.* **2020**, *604* (April), 117786.

(13) Ding, Y.; Gao, Q.; Li, G.; Zhang, H.; Wang, J.; Yan, L.; Suo, J. Selective Epoxidation of Cyclohexene to Cyclohexene Oxide Catalyzed by Keggin-Type Heteropoly Compounds Using Anhydrous Urea-Hydrogen Peroxide as Oxidizing Reagent and Acetonitrile as the Solvent. *J. Mol. Catal. A Chem.* **2004**, *218* (2), 161−170.

(14) Ishikawa, E.; Yamase, T. Kinetics of Epoxidation of Cyclooctene with H2O2 by α-Keggin $[PTi_2W_{10}O_{38}(O_2)_2]^{7-}$ Catalyst in Acetonitrile. *J. Mol. Catal. A Chem.* **1999**, *142* (1), 61−76.

(15) Hua, L.; Qiao, Y.; Li, H.; Feng, B.; Pan, Z.; Yu, Y.; Zhu, W.; Hou, Z. Epoxidation of Olefins with Hydrogen Peroxide Catalyzed by a Reusable Lacunary-Type Phosphotungstate Catalyst. *Sci. China Chem.* **2011**, *54* (5), 769−773.

(16) Vilanculo, C. B.; da Silva, M. J. Can Brønsted Acids Catalyze the Epoxidation of Allylic Alcohols with H_2O_2? With a Little Help from the Proton, the $H_3PMo_{12}O_{40}$ Acid Did It and Well. *Mol. Catal.* **2021**, *512* (July), 111780.

(17) Neumann, R.; Levin, M. Aerobic Oxidative Dehydrogenations Catalyzed by the Mixed-Addenda Heteropolyanion $PV_2Mo_{10}O_{40}^{5-}$: A Kinetic and Mechanistic Study. *J. Am. Chem. Soc.* **1992**, *114* (18), 7278−7286.

(18) Ishii, Y.; Yamawaki, K.; Yoshida, T.; Ura, T.; Ogawa, M. Oxidation of Olefins and Alcohols by Peroxo-Molybdenum Complex Derived from Tris(Cetylpyridinium) 12-Molybdophosphate and Hydrogen Peroxide. *J. Org. Chem.* **1987**, *52* (9), 1868−1870.

(19) Sathicq, Á. G.; Pizzio, L. R.; Vázquez, P. G.; Tundo, P.; Aricò, F.; Romanelli, G. P. Keggin Heteropolyacid as Catalyst for Olefin Epoxidation: A Multiphase Approach. *Sustain. Chem. Pharm.* **2020**, *15* (257), 100201.

(20) Ishii, Y.; Yamawaki, K.; Ura, T.; Yamada, H.; Yoshida, T.; Ogawa, M. Hydrogen Peroxide Oxidation Catalyzed by Heteropoly Acids Combined with Cetylpyridinium Chloride. Epoxidation of Olefins and Allylic Alcohols, Ketonization of Alcohols and Diols, and Oxidative Cleavage of 1,2-Diols and Olefins. *J. Org. Chem.* **1988**, *53* (15), 3587−3593.

(21) Duncan, D. C.; Chambers, R. C.; Hecht, E.; Hill, C. L. Mechanism and Dynamics in the $H_3[PW_{12}O_{40}]$-Catalyzed Selective

Epoxidation of Terminal Olefins by H2O2. Formation, Reactivity, and Stability of $\{PO_4[WO(O_2)_2]_4\}^{3-}$. *J. Am. Chem. Soc.* **1995**, *117* (2), 681−691.
(22) Yamase, T.; Ishikawa, E.; Asai, Y.; Kanai, S. Alkene Epoxidation by Hydrogen Peroxide in the Presence of Titanium-Substituted Keggin-Type Polyoxotungstates $[PTi_xW_{12-X}O_{40}]^{(3+2x)-}$ and $[PTi_xW_{12-X}O_{40-x}(O_2)_x]^{(3+2x)-}$ (x = 1 and 2). *J. Mol. Catal. A Chem.* **1996**, *114* (1−3), 237−245.
(23) Wang, S.-S.; Liu, W.; Wan, Q.-X.; Liu, Y. Homogeneous Epoxidation of Lipophilic Alkenes by Aqueous Hydrogen Peroxide: Catalysis of a Keggin-Type Phosphotungstate-Functionalized Ionic Liquid in Amphipathic Ionic Liquid Solution. *Green Chem.* **2009**, *11* (10), 1589.
(24) Taghiyar, H.; Yadollahi, B. New Perspective to Catalytic Epoxidation of Olefins by Keplerate Containing Keggin Polyoxometalates. *Polyhedron* **2018**, *156*, 98−104.
(25) Kuzminska, M.; Kovalchuk, T. V.; Backov, R.; Gaigneaux, E. M. Immobilizing Heteropolyacids on Zirconia-Modified Silica as Catalysts for Oleochemistry Transesterification and Esterification Reactions. *J. Catal.* **2014**, *320* (1), 1−8.
(26) Xiaoxiang, H.; Yingying, K.; Chunhua, X.; Xiujuan, T.; Qing, C.; Kuiwu, W.; Chin-Te, H.; Li-Li, L.; Shang-Bin, L. Heteropoly Tungstate Supported on Metal Oxide Catalysts for Liquid Phase Oxidation of Benzyl Alcohol with Hydrogen Peroxide. *J. Braz. Chem. Soc.* **2017**, *29* (1), 88−98.
(27) Cohen, M.; Neumann, R. Silica Tethered with Poly(Ethylene and/Propylene) Oxide as Supports for Polyoxometalates in Catalytic Oxidation. *J. Mol. Catal. A Chem.* **1999**, *146* (1−2), 291−298.
(28) Ghubayra, R.; Nuttall, C.; Hodgkiss, S.; Craven, M.; Kozhevnikova, E. F.; Kozhevnikov, I. V. Oxidative Desulfurization of Model Diesel Fuel Catalyzed by Carbon-Supported Heteropoly Acids. *Appl. Catal. B Environ.* **2019**, *253* (April), 309−316.
(29) Batalha, D. C.; Ferreira, S. O.; Silva, R. C.; Silva, M. J. Cesium-Exchanged Lacunar Keggin Heteropolyacid Salts: Efficient Solid Catalysts for the Green Oxidation of Terpenic Alcohols with Hydrogen Peroxide. *ChemistrySelect* **2020**, *5* (6), 1976−1986.
(30) Masteri-Farahani, M.; Modarres, M. Encapsulation of Keggin-Type Phosphotungstic Acid into the Mesopores of SBA-16 as a Reusable Heterogeneous Catalyst for the Epoxidation of Olefins. *Sci. Iran.* **2017**, *24* (6), 0.
(31) Vilanculo, C. B.; da Silva, M. J.; Rodrigues, A. A.; Ferreira, S. O.; da Silva, R. C. Vanadium-Doped Sodium Phosphomolybdate Salts as Catalysts in the Terpene Alcohols Oxidation with Hydrogen Peroxide. *RSC Adv.* **2021**, *11* (39), 24072−24085.
(32) Villabrille, P.; Romanelli, G.; Vázquez, P.; Cáceres, C. Vanadium-Substituted Keggin Heteropolycompounds as Catalysts for Ecofriendly Liquid Phase Oxidation of 2,6-Dimethylphenol to 2,6-Dimethyl-1,4-Benzoquinone. *Appl. Catal. A Gen.* **2004**, *270* (1−2), 101−111.
(33) Han, Q.; He, C.; Zhao, M.; Qi, B.; Niu, J.; Duan, C. Engineering Chiral Polyoxometalate Hybrid Metal-Organic Frameworks for Asymmetric Dihydroxylation of Olefins. *J. Am. Chem. Soc.* **2013**, *135* (28), 10186−10189.
(34) Qiu, J.; Wang, G.; Zeng, D.; Tang, Y.; Wang, M.; Li, Y. Oxidative Desulfurization of Diesel Fuel Using Amphiphilic Quaternary Ammonium Phosphomolybdate Catalysts. *Fuel Process. Technol.* **2009**, *90* (12), 1538−1542.
(35) Swalus, C.; Farin, B.; Gillard, F.; Devillers, M.; Gaigneaux, E. M. Hybrid Peroxotungstophosphate Organized Catalysts Highly Active and Selective in Alkene Epoxidation. *Catal. Commun.* **2013**, *37*, 80−84.
(36) Nadealian, Z.; Mirkhani, V.; Yadollahi, B.; Moghadam, M.; Tangestaninejad, S.; Mohammadpoor-Baltork, I. Green and Efficient Oxidation of Benzylic Alcohols with Hydrogen Peroxide Catalyzed by an Inorganic-Organic Hybrid Catalyst. *J. Coord. Chem.* **2013**, *66* (7), 1264−1275.
(37) Li, X.; Cao, R.; Lin, Q. Solvent-Free Baeyer-Villiger Oxidation with H2O2 as Oxidant Catalyzed by Multi-SO3H Functionalized Heteropolyanion-Based Ionic Hybrids. *Catal. Commun.* **2015**, *63*, 79−83.
(38) Leng, Y.; Liu, J.; Jiang, P.; Wang, J. POSS-Derived Mesostructured Amphiphilic Polyoxometalate-Based Ionic Hybrids as Highly Efficient Epoxidation Catalysts. *ACS Sustain. Chem. Eng.* **2015**, *3* (1), 170−176.
(39) Xue, S.; Chen, G.; Long, Z.; Zhou, Y.; Wang, J. Efficient and Recyclable Multi-Cationic Polyoxometalate-Based Hybrid Catalyst for Heterogeneous Cyclohexane Oxidation with H_2O_2. *RSC Adv.* **2015**, *5* (25), 19306−19314.
(40) Mirante, F.; Dias, L.; Silva, M.; Ribeiro, S. O.; Corvo, M. C.; de Castro, B.; Granadeiro, C. M.; Balula, S. S. Efficient Heterogeneous Polyoxometalate-Hybrid Catalysts for the Oxidative Desulfurization of Fuels. *Catal. Commun.* **2018**, *104*, 1−8.
(41) Mimoun, H.; Seree de Roch, I.; Sajus, L. Epoxydation Des Olefines Par Les Complexes Peroxydiques Covalents Du Molybdene-VI. *Tetrahedron* **1970**, *26* (1), 37−50.
(42) Mimoun, H. The Role of Peroxymetallation in Selective Oxidative Processes. *J. Mol. Catal.* **1980**, *7* (1), 1−29.
(43) Sharpless, K. B.; Townsend, J. M.; Williams, D. R. Mechanism of Epoxidation of Olefins by Covalent Peroxides of Molybdenum(VI). *J. Am. Chem. Soc.* **1972**, *94* (1), 295−296.
(44) Deubel, D. V.; Sundermeyer, J.; Frenking, G. Mechanism of the Olefin Epoxidation Catalyzed by Molybdenum Diperoxo Complexes: Quantum-Chemical Calculations Give an Answer to a Long-Standing Question. *J. Am. Chem. Soc.* **2000**, *122* (41), 10101−10108.
(45) Hidalgo, G.; Barozzino-Consiglio, G.; Devillers, M.; Gaigneaux, E. M. Active Epoxidation Bipyridine-Oxodiperoxotungstate Catalysts. *Mol. Catal.* **2022**, *528*, 112479.
(46) Hidalgo, G.; Devillers, M.; Gaigneaux, E. M. Hybrid Materials Based on Keggin Phosphotungstate and Bipyridine with Valuable Hydrophobic and Redox Properties. *Inorg. Chem.* **2022**, *61* (32), 12494−12507.
(47) Moissette, A.; Batonneau, Y.; Brémard, C. Conformation and Protonation of 2,2′-Bipyridine and 4,4′-Bipyridine in Acidic Aqueous Media and Acidic ZSM-5 Zeolites: A Raman Scattering Study. *J. Am. Chem. Soc.* **2001**, *123* (49), 12325−12334.
(48) Barker, D. J.; Summers, L. A.; Cooney, R. P. Conformations of 2,2′-Bipyridine in Acidic Media. *J. Mol. Struct.* **1987**, *159* (3−4), 249−254.
(49) Okuhara, T.; Mizuno, N.; Misono, M. Catalytic Chemistry of Heteropoly Compounds. *Adv. Catal.* **1996**, *41* (C), 113−252.
(50) Rocchiccioli-Deltcheff, C.; Thouvenot, R.; Franck, R. Spectres i.r. et Raman d'hétéropolyanions α-$XM_{12}O_{40}^{n-}$ de Structure de Type Keggin (X = B^{III}, Si^{IV}, Ge^{IV}, P^{V}, As^{V} et M = W^{VI} et Mo^{VI}). *Spectrochim. Acta Part A Mol. Spectrosc.* **1976**, *32* (3), 587−597.
(51) Strukl, J. S.; Walter, J. L. Infrared and Raman Spectra of Heterocyclic Compounds-III. The Infrared Studies and Normal Vibrations of 2,2′-Bipyridine. *Spectrochim. Acta Part A Mol. Spectrosc.* **1971**, *27* (2), 209−221.
(52) Parker, L. M.; Bibby, D. M.; Burns, G. R. Fourier-Transform Infrared Study of Pyridine Sorbed on Zeolite HY. *J. Chem. Soc. Faraday Trans.* **1991**, *87* (19), 3319−3323.
(53) Kamyshny, A. L.; Zakharov, V. N.; Fedorov, Y. V.; Galashin, A. E.; Aslanov, L. A. Surface-Enhanced Raman Scattering of 2,2′-Bipyridine Adsorbed on Colloidal Silver and Stabilized AgBr Sols. *J. Colloid Interface Sci.* **1993**, *158* (1), 171−182.
(54) Brolo, A. G.; Jiang, Z.; Irish, D. E. The Orientation of 2,2′-Bipyridine Adsorbed at a SERS-Active Au(1 1 1) Electrode Surface. *J. Electroanal. Chem.* **2003**, *547* (2), 163−172.
(55) Yan, Q. X.; Shen, Y.; Niu, J. Y.; Wang, J. P. The Hydrothermal Synthesis and Crystal Structure of $[2.2'\text{-BipyH}]_3PW_{12}O_{40}$. *Russ. J. Inorg. Chem.* **2009**, *54* (6), 930−934.
(56) Amarante, T. R.; Antunes, M. M.; Valente, A. A.; Paz, F. A. A.; Pillinger, M.; Gonçalves, I. S. Crystal Structure and Catalytic Behavior in Olefin Epoxidation of a One-Dimensional Tungsten Oxide/Bipyridine Hybrid. *Inorg. Chem.* **2015**, *54* (20), 9690−9703.

https://doi.org/10.1021/acs.inorgchem.3c00467
Inorg. Chem. XXXX, XXX, XXX−XXX

(57) Schlemper, E. O.; Schrauzer, G. N.; Hughes, L. A. Crystal Structure of Oxo(Diperoxo)Bipyridylmolybdenum(VI). *Polyhedron* **1984**, *3* (3), 377−380.
(58) Speca, A. N.; Pytlewski, L. L.; Karayannis, N. M.; Owens, C. 2,2′-Bipyridine n-Oxide and 1,10-Phenanthroline n-Oxide Complexes with Divalent 3d Metal Nitrates. *J. Inorg. Nucl. Chem.* **1974**, *36* (12), 3751−3761.
(59) Ohsawa, Y.; DeArmond, M. K.; Hanck, K. W.; Moreland, C. G. A Proton NMR Study of Reduced Paramagnetic Tris(2,2'-Bipyridine) Complexes of Iron(II), Ruthenium(II) and Osmium(II). *J. Am. Chem. Soc.* **1985**, *107* (19), 5383−5386.
(60) Simándi, L. I. *Catalytic Oxidations with Hydrogen Peroxide as Oxidant*; Strukul, G., Ed.; Catalysis by Metal Complexes, Springer Netherlands: Dordrecht, 1992; Vol. *9*.
(61) Thiel, W. R. Metal Catalyzed Oxidations. Part 5. Catalytic Olefin Epoxidation with Seven-Coordinate Oxobisperoxo Molybdenum Complexes: A Mechanistic Study11For Part 4 of the Series: See [1]. *J. Mol. Catal. A Chem.* **1997**, *117* (1−3), 449−454.
(62) Thiel, W. R.; Barz, M.; Glas, H.; Pleier, A.-K. Olefin Epoxidation Catalyzed by Molybdenum Peroxo Complexes: A Mechanistic Study. *Peroxide Chemistry: Mechanistic and Preparative Aspects of Oxygen Transfer*; Wiley-VCH Verlag GmbH, 2000; Chapter 7..
(63) Hidalgo Gutierrez, G. Hybridization of Keggin polyoxometalates for epoxidation catalysis. Ph.D. thesis, UCLouvain (Belgium), 2022. http://hdl.handle.net/2078.1/271191.

https://doi.org/10.1021/acs.inorgchem.3c00467
Inorg. Chem. XXXX, XXX, XXX−XXX